DFT Investigation of Intermediate Steps in the Hydrolysis of α-Al_2O_3(0001)†

Víctor A. Ranea,‡,§,|| Ian Carmichael,‡,⊥ and William F. Schneider*,§,⊥

Radiation Laboratory, University of Notre Dame, Notre Dame, Indiana 46556, Department of Chemical and Biomolecular Engineering, University of Notre Dame, Notre Dame, Indiana 46556, Instituto de Investigaciones Físico-Químicas Teóricas y Aplicadas (CONICET) Facultad de Ciencias Exactas, Universidad Nacional La Plata, Argentina, Department of Chemistry and Biochemistry, University of Notre Dame, Notre Dame, Indiana 46556

Received: August 05, 2008; Revised Manuscript Received: October 15, 2008

The α-Al_2O_3(0001) surface is well-known to become hydroxylated in the presence of water, and this hydroxylation is important to subsequent alumina surface chemistry. Here, we use plane-wave, supercell density functional theory to examine the progression of multiple water dissociation steps from the hydrogen-free stoichimetric surface to the fully hydroxylated, gibbsite-like surface. Consistent with earlier reports, we find that water molecules adsorb and dissociate exothermically and with a small activation barrier at unhydroxylated and coordinatively unsaturated surface Al_s sites and that the formation energy of these hydroxylated Al_s is coverage-independent. Subsequent water dissociations at a singly hydroxylated Al_s site, steps necessary to liberate Al_s and reach the fully hydroxylated surface, are approximately thermoneutral at any surface hydroxyl coverage. Further, within the pathways we are able to identify, these subsequent dissociation steps proceed along more complex reaction coordinates and have higher activation energies than the first water dissociation step. Although the fully hydroxylated surface is the thermodynamic ground state in the presence of water, the actual α-Al_2O_3(0001) surface composition under any particular conditions may exhibit strong dependence on sample history.

1. Introduction

Because of their relevance to the many technological use of oxides, to material corrosion, and to the behavior of minerals in the environment, the reactions of water with metal oxide surfaces remain a topic of considerable scientific discussion.[1−5] Aluminum oxide (alumina, Al_2O_3) is particularly interesting in this respect. Alumina is a common and technologically important base metal oxide, finding use in electronic materials, as a high surface area support for catalytic metal particles, as a ceramic, and appearing in many forms in the environment. Alumina exists in a variety of polymorphs,[6] and the existence of many metastable transitional aluminas that incorporate some amount of bulk hydroxyl groups suggests the existence of a rich surface chemistry with water.[7]

Corundum, or α-Al_2O_3, is the most stable form of bulk alumina. Its crystal structure consists of a hexagonal array of oxygen anions with aluminum cations in octahedral holes.[8] Under ultrahigh vacuum conditions, the nonpolar, Al-terminated (0001) surface, which exposes 3-fold coordinated Al_s, is found in both experiment and simulation to minimize the surface energy.[9−16] There is also general agreement that this "dry," or H-free, alumina surface readily reacts with water to form surface hydroxyls,[17−25] but the exact nature and progression of this hydrolysis process is not clear. Initial hydroxyl formation at low exposures of water have been attributed to reactions at surface defects. Higher water exposures result in hydroxylation of the basal plane,[17−20,24] as indicated by calorimetric,[17,18,26] thermal desorption,[19] photoemission,[20] and vibrational spectroscopic[24,25] experiments.

Electronic structure simulations, primarily based on density functional theory (DFT), describe the first step in basal plane hydroxylation as water dissociation across one of three equivalent Al_s-O_s surface bonds, as shown in the first step below:[21,22,27−29] The resulting Al_s-hydroxylated surface exposes

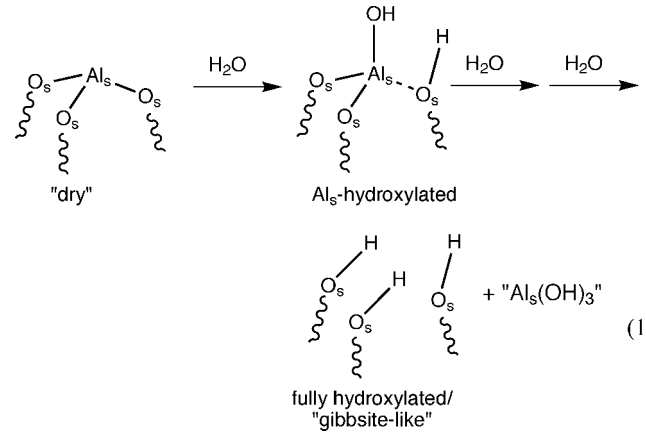

(1)

two types of surface hydroxyls above a plane of 4-fold coordinated Al. Car−Parrinello molecular dynamics (CPMD) DFT simulations show that this initial dissociation step has a small activation barrier and occurs rapidly at ambient temperatures.[21,22] The calculated dissociation energetics are further found to be consistent with water chemisorption energies observed in microcalorimetry experiments on low surface area corundum.[18]

The structure of the corundum surface at higher water exposures has been studied using crystal truncation rod diffraction and is found to expose exclusively a subsurface of

† Part of the special section "Physical Chemistry of Environmental Interfaces".

* Corresponding author. E-mail: wschneider@nd.edu.
‡ Radiation Laboratory, University of Notre Dame.
§ Department of Chemical and Biomolecular Engineering, University of Notre Dame.
|| Universidad Nacional La Plata.
⊥ Department of Chemistry and Biochemistry, University of Notre Dame.

10.1021/jp8069892 CCC: $40.75
Published on Web 01/05/2009

octahedral Al and to be nominally O-terminated.[23] This surface composition can be rationalized as the culmination of multiple water dissociations, as shown schematically in eq 1, above, that liberate the top layer of Al as some form of bulk or soluble hydroxide and leave behind a hydroxyl-covered surface[11,21,23] that resembles gibbsite, or $Al(OH)_3$. CPMD simulations reveal this fully hydroxylated surface to possess a dynamic layer of in-plane and out-of-plane hydroxyl groups and a vibrational spectrum consistent with experimental observation.[21,22] This surface composition is also consistent with first-principles thermodynamic modeling that shows the fully hydroxylated (0001), or "gibbsite-like," surface to minimize the alumina surface free energy under all but the most dry conditions.[11−14,16,29]

Although the inital water dissociation step and equilibrium composition of α-Al_2O_3(0001) in the presence of water have received a great deal of attention, there has been little work on the intermediate steps and states of surface reaction with water. The transition from the dry to Al_s-hydroxylated to fully hydroxylated surfaces shown in eq 1 entails the breaking of multiple surface Al_s-O_s bonds and ultimately the formation of $Al_s(OH)_3$, which may remain at or be transported from the surface, depending on experimental conditions. Neither the energetics nor the kinetics of these steps have been examined; neither has the possible role of molecular water in stabilizing intermediate surface states. Here, we address this gap using DFT simulation. We consider a set of water adsorption and dissociation intermediates and steps along the path from the dry to fully hydroxylated surface, including the influence of surface coverage on their stability. We find that the thermodynamic driving force for forming intermediate hydroxylated states is small and that the barrier to water dissociation events on the basal plane becomes increasingly large with increasing hydroxyl coverage. The results suggest a complex and kinetically limited transition between the dry and the fully hydroxylated alumina basal plane.

2. Computational Details

First-principles total energy calculations were performed within a plane-wave, supercell, density functional theory (DFT) framework using the Vienna Ab Initio Simulation Package.[30,31] Electron exchange and correlation energies were calculated within the generalized gradient approximation (GGA) in the Perdew−Wang 91 form.[32] The Kohn−Sham equations were solved using the projector augmented wave (PAW) approach for describing electronic core states[33,34] and a basis set including plane waves up to 400 eV. Self-consistent energies are converged to 0.1 meV, and ionic relaxations are considered converged when the forces on the ions are less than 0.03 eV/Å.

Within the approximations used here, the calculated bulk corundum lattice constants are $a = 4.806$ and $c = 13.119$ Å, consistent with other reports. Following previous work,[35] the (0001) surface is described by a 12-layer-thick slab (four complete $Al(O_3)Al$ layers) containing two unit cells in the lateral directions (Figure 1). The first Brillouin zone of the hexagonal supercell was sampled with a $(3 \times 3 \times 1)$ Γ-centered mesh, including five symmetry unique **k**-points. The seven topmost ionic layers and any adsorbates were allowed to relax, and the five bottom layers were kept fixed at their optimized bulk positions. To avoid unphysical interlayer interactions, the slabs were separated by a vacuum region of 17.98 Å.

Unless otherwise stated, adsorption energies are calculated by difference in GGA energy among isolated, molecular water; the relaxed (0001) α-Al_2O_3 supercell; and the relaxed, adsorbed water state. We used the climbing image nudged elastic band (CI-NEB) method to calculate the minimum energy paths (MEP) and transition states for several water dissociation steps.[36,37] After construction of an initial guess MEP using linear interpolation between reactant and product states, an initial NEB calculation was performed to locate the MEP. A subsequent CI-NEB calculation was used to force one image to the transition state, which was converged to 0.03 eV/Å. The Hessian matrix of second derivatives was determined for all ground and transition state structures within the harmonic approximation by two-sided finite differences, using a displacement step of 0.01 Å. All adsorbate atoms and the outermost Al and O layers ions were displaced in these calculations, and diagonalization of the dynamical matrix yields the harmonic frequencies. Ground and transtion states contained zero and one imaginary frequency, respectively. The harmonic DFT vibrational frequencies systematically overestimate real anharmonic frequencies.[38] Within the approximations used here, the two H−O stretches in gas-phase water are overestimated by 1.375%, and we correct all our reported hydroxyl vibrational frequencies using this scale factor.

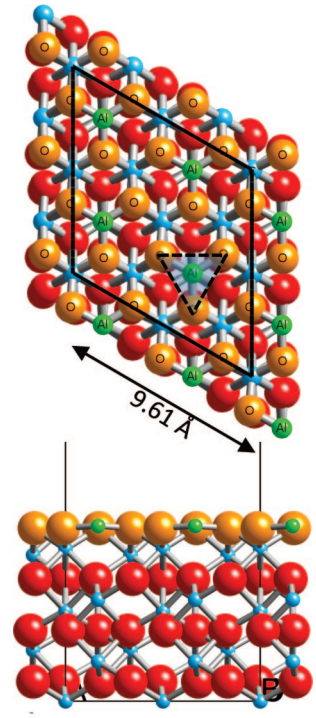

Figure 1. Top and side views of the 2×2 (0001) α-Al_2O_3 supercell. Al are indicated by small blue and green (Al_s) spheres, and O, by large red and orange (O_s) spheres. Triangle indicates $Al_sO_{s,3}$ water dissociation site.

3. Results

3.1. Initial Water Dissociation States. As noted above, the lowest energy, stoichiometric α-Al_2O_3(0001) surface exposes a top layer of surface Al_s cations and a hexagonal array of second-layer O_s anions. In the relaxed, adsorbate-free surface, Al_s (green spheres, Figure 1) relax toward the O_s (orange spheres) plane, decreasing the interlayer spacing to ≈0.10 Å and creating a nearly trigonal environment of O_s around Al_s. The Al_s-O_s bonds are all equivalent and have a calculated length of 1.703 Å, whereas O_s bind to the two subsurface Al layers with distances of 1.820 and 1.905 Å, respectively.

The Al_s possess vacant, out-of-plane 2p orbitals that make them Lewis acidic adsorption sites. A single, isolated water molecule is calculated at the GGA level to molecularly adsorb to these sites through its O atom, parallel to the surface, with a binding energy of 1.14 eV (Figure 2a).[35] Water adsorption draws

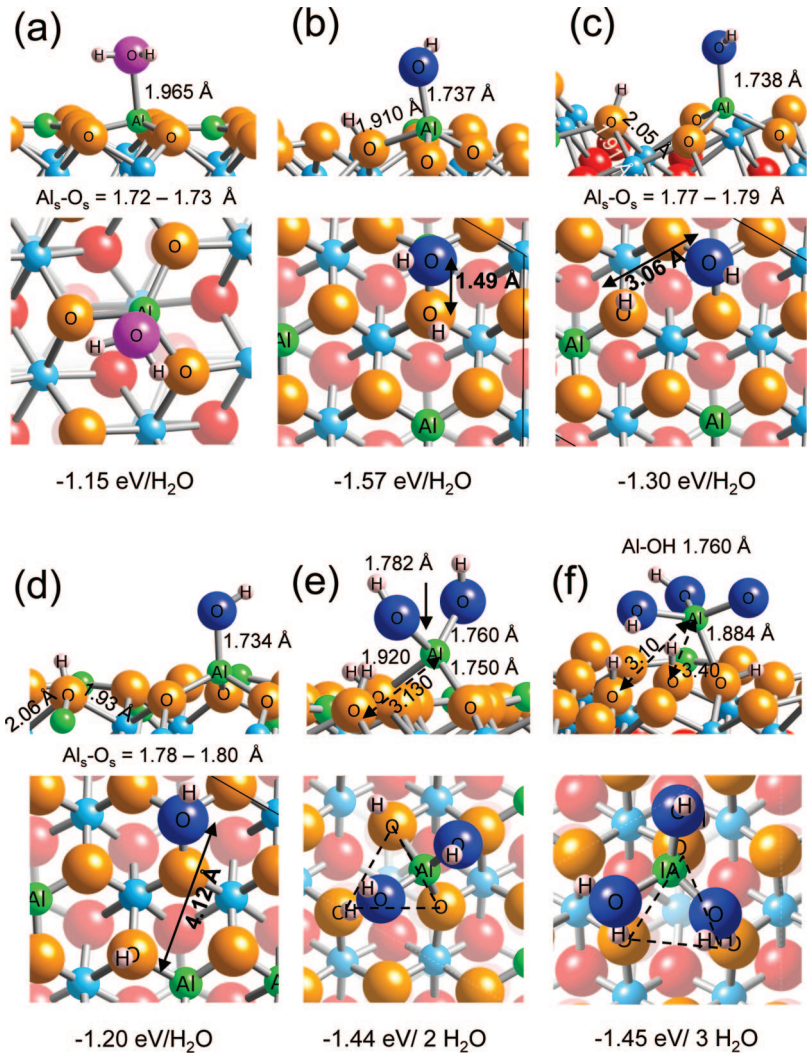

Figure 2. Top and side views of isolated water adsorption states: (a) molecularly adsorbed water, (b) 1−2 dissociated water, (c) nearer 1−4 dissociated water, (d) further 1−4 dissociated water, (e) 1−2 dissociated water pair, and (f) 1−2 dissociated water triple. Orange-, magenta-, and dark blue-labeled spheres indicate O_s, molecular water O, and dissociated water O, respectively. Unlabeled spheres belong to subsurface atoms.

up Al_s slightly, increasing the Al_s-O_s distance 0.03 Å and creating a flattened tetrahedral environment about Al_s. The O_s anion sites are Lewis basic and also contribute to water binding at higher coverages. A molecular water layer is found to saturate at $2H_2O/Al_s$, with half the water bound through O to Al_s and the other half bound through H to O_s, forming a hexagonal, hydrogen-bonded water "bilayer" above the alumina plane (Figure 3a).[35] The average molecular water binding energy is calculated to be approximately constant across these two limits of water coverage.

These molecular water states are metastable to dissociated water. As shown in eq 1, above, the preferred mode of isolated water dissociation is to an OH fragment atop Al and H fragment atop O_s.[11,21,22,27−29] We explored the structure and energetics of the isolated monohydroxylated state as a function of relative binding locations of H and OH fragments (Figure 2b−d). An attractive interaction between H and OH favors 1−2 dissociation across a connected Al_s-O_s fragment, and dissociation is exothermic with respect to gas-phase or adsorbed water.

$$Al_sO_{s,3} + H_2O \rightarrow (HO)Al_sO_{s,2} + O_sH \quad \Delta E_1 = -1.57 \text{ eV} \tag{2}$$

This absolute adsorption energy is slightly (0.2 eV) more negative than that calculated using an ab initio embedded cluster model[28] or within an earlier, smaller, and less tightly converged supercell model,[21] differences within the range expected for these different computational models. As with molecular water adsorption, dissociation again draws Al_s away from the surface plane and into a flattened tetrahedral coordination environment, but now in which two Al_s-O_s and the Al_s-OH bonds are of comparable length and the Al_s-O_sH separation is increased to 1.91 Å. This 1−2 dissociation generates two types of surface hydroxyls at the expensive of a lengthened and weakened Al_s-O_sH bond.

Moving the H atom to a next-nearest-neighbor 1−4 position (Figure 2c) is found to decrease the adsorption energy by 0.27 eV to −1.30 eV with respect to gas-phase water. The coordination environment about the Al adsorption site becomes more regularly tetrahedral, with four approximately equivalent Al−O bonds, while the protonated O_s relaxes away from its neighbor Al_s to 1.84 Å. Similar relaxations are found at the third-nearest-neighbor 1−4 separation (Figure 2d), along with a further decrease in adsorption energy to −1.20 eV. The energy penalty with increasing lateral separation has been noted previously.[22] It reflects the electrostatic interaction between the nominally Al_s-OH^- and O_s-H^+ products of heterolytic water dissociation, similar to that which underlies the "cooperative" interaction between Lewis acidic and basic adsorbates noted on other

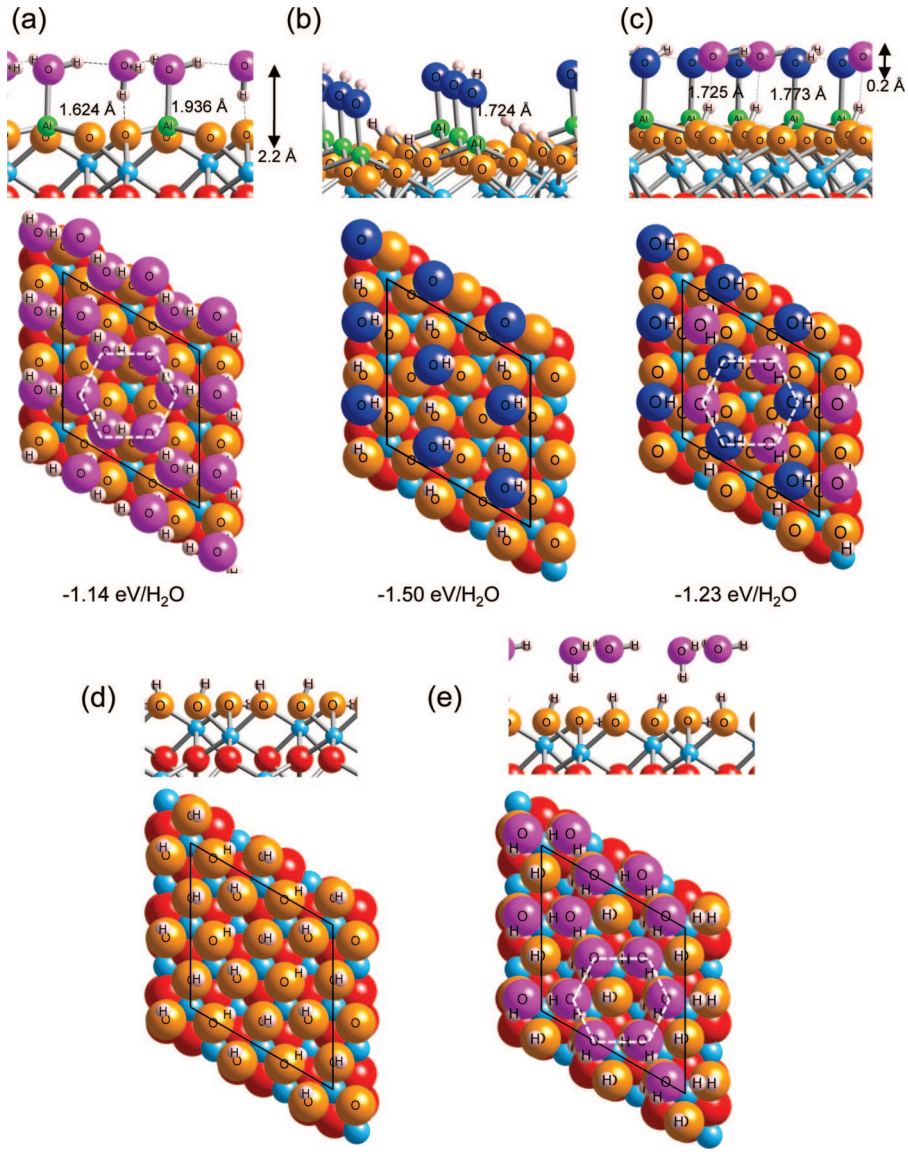

Figure 3. Top and side views of saturation coverage water adsorption states: (a) molecular water bilayer, (b) monolayer Al_s-hydroxylated surface, (c) monolayer Al_s-hydroxylated surface with molecular water, (d) fully hydroxylated, "gibbsite-like" surface, and (e) fully hydroxylated surface with molecular water overlayer. In color version, orange, magenta, and dark blue labeled spheres indicate O_s, molecular water O, and dissociated water O, respectively. Unlabeled spheres belong to subsurface atoms.

oxides.[39,40] At infinite H and OH separation, (i.e., adsorbates calculated in separate supercells), the dissociative water adsorption energy increases to 0.25 eV endothermic.

Previous molecular dynamics and transition state calculations predict dissociation of molecularly adsorbed water to the 1−2 chemisorbed state to have a modest barrier (<0.4 eV).[21,22,27] Figure 4 shows the CI-NEB minimum energy dissociation pathway calculated within the GGA. The transition state structural features are entirely consistent with earlier reports; the absolute transition state energy (0.19 eV) is slightly lower than the B3LYP energy within a cluster model[27] or the free energy from potential of mean force calculations.[21,22] All these results are consistent with facile 1−2 dissociation of water on the (0001) basal plane.

The results above correspond to a 1/4 ML coverage of dissociated water within our 2 × 2 supercell model. We find additional dissociations of water at unreacted Al_s to proceed with comparable energy and to produce similar local relaxations. Consistent with the 1/4 ML results, 1−2 dissociation is strongly preferred at all coverages; that is, configurations in which H and OH fragments are located on adjacent O_s and Al_s are energetically favored. As shown in Figure 1, each Al_s has three neighbor O_s so that various orderings of H fragments are possible even within the constraint of one H/OH pair per Al_s. We find this H configurational ordering to have a negligible effect on adsorption energies. The 1 × 1 ordered H/OH configuration is shown in Figure 3b. The average water binding energy at this coverage decreases modestly to −1.5 eV/H_2O from the 1/4 ML value, comparable to a previous report.[29]

This monolayer-covered surface of hydroxylated Al_s can accommodate additional molecular water. In analogy to the molecular water bilayer (Figure 3a), we find that molecular water completes a hexagonal network of hydrogen-bonded water and hydroxyl groups, with molecular water O situated atop protonated O_s sites (Figure 3c). This network is similar to that found to spontaneously form and to promote water dissociation in CPMD simulations of the (0001) surface dosed with molecular water.[21] The average adsorption energy of this mixed dissociated and molecular state decreases to −1.23 eV/H_2O, which corresponds to adsorption of the molecular water fraction with a

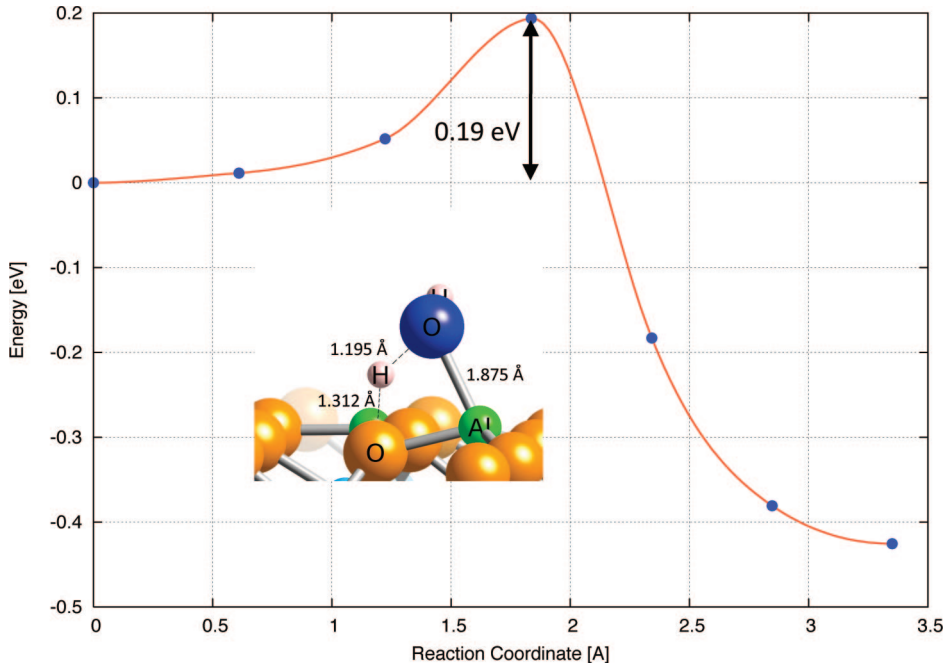

Figure 4. Climbing image NEB-calculated 1−2 water dissociation pathway at an isolated Al_s-O_s site. Inset shows transition state structure. Unscaled $\nu_{TS}^{\ddagger} = 854i\ cm^{-1}$.

binding energy of ≈1 eV/H_2O. Microcalorimetry experiments show the average water adsorption energy to decline as surface hydroxylation approaches monolayer saturation of 10 OH/nm on the basal plane.[17] A possible interpretation of this decrease is the simultaneous adsorption of dissociated and molecular water into this mixed state. In fact, the 0.3 eV/H_2O energy difference between a single dissociated water molecule and mixed dissociated and molecular state is identical to the observed linear decline in binding energy with increasing basal plane coverage. The presence of both molecular and dissociated water is also consistent with vibrational spectroscopy observations at moderate water dosages.[24]

3.2. Intermediate Water Dissociation States. The completely Al-hydroxylated surface leaves 2/3 of the Al_s-O_s bonds unreacted and potentially available to dissociate waters; cleavage of all of these bonds is, in principle, necessary to generate the fully hydroxylated surface. Figure 2e shows the product of 1−2 dissociation of a second water at a monohydroxylated (HO)$AlO_{s,2}$ site. The final configuration retains 4-fold O coordination around Al, but with Al_s raised up from the surface plane and displaced 1.12 Å to a position approximately bridging two O_s. The formation of a second Al_s-OH bond thus comes at the expense of one Al_s-O_sH interaction, which increases in separation to 3.13 Å. As with the first water dissociation, the reacting Al_s center has three short Al−O bonds (here, two to OH and one to the remaining unprotonated O_s) plus a fourth, longer dative bond to a nearest-neighbor protonated O_sH. Both O_s-bound protons adopt configurations that point away from the surface plane.

The formation energy of an isolated $(HO)_2Al_sO_s$ site with respect to the dry surface and two molecular waters is calculated to be −1.44 eV so that the net addition of the second water is slightly endothermic.

$$(HO)Al_sO_{s,2} + H_2O \rightarrow (HO)_2Al_sO_s + O_sH \quad \Delta E_2 = 0.13\ eV \tag{3}$$

These energetics become even more unfavorable if the reference state is molecular water adsorbed on a vacant Al_s site or within an overlayer of water (Figure 3c). There is thus a strong energetic preference for Al_s monohydroxylation (reaction 2) over dihydroxylation (reaction 3). Because the monohydroxylation energy is nearly coverage-independent, the monohydroxylated layer is favored to be completed before formation of any dihydroxylated sites. As a further check, we calculated the formation energy of a dihydroxylated $(HO)_2Al_sO_s$ site on the monolayer monohydroxylated surface. The local structure of the dihydroxylated site is essentially the same within the two models, whereas the energy of reaction 3 decreases 0.5 to −0.34 eV. Similar energies are found for formation of higher coverages of dihydroxlated sites. The energetics of dihydroxylation, thus, are somewhat sensitive to the surface hydroxyl coverage, but at all coverages, the first water dissociation event is much more favorable than the second, and the second event is endothermic with respect to molecularly adsorbed water.

Constructing a pathway for this second water dissociation proves more complicated than that for the first. In analogy to Figure 4, we considered a pathway beginning from molecular water adsorbed at an $(HO)Al_sO_{s,2}$ site, proceeding through a 1,2 dissociation, and ending with the dihydroxylated site. As shown at the left side of Figure 5, structure a, we were able to locate an adsorbed molecular water configuration that is bound by about −0.5 eV. The Al_s and five nearest-neighbor oxygens form an approximate trigonal bipyramid in this structure, with two Al_s-O_s and the Al_s-OH bonds at the equator, water at one axial end, and O_s-H at the other. The relatively weak water binding energy compared to those noted above reflects the energetic cost of rehybridizing the Al_s center and suggests that this water adsorption step may have some activation barrier. Because the entrance configuration for this water adsorption event is not evident, we did not attempt to calculate a barrier.

A candidate reaction path was constructed from this initial adsorbed water structure to the final dihydroxylated state. Multiple minimums appeared in preliminary NEB calculations, and further optimizations identified a higher-energy molecular water configuration, structure b in Figure 5, in which one water proton is reoriented to more closely approach the nearest-

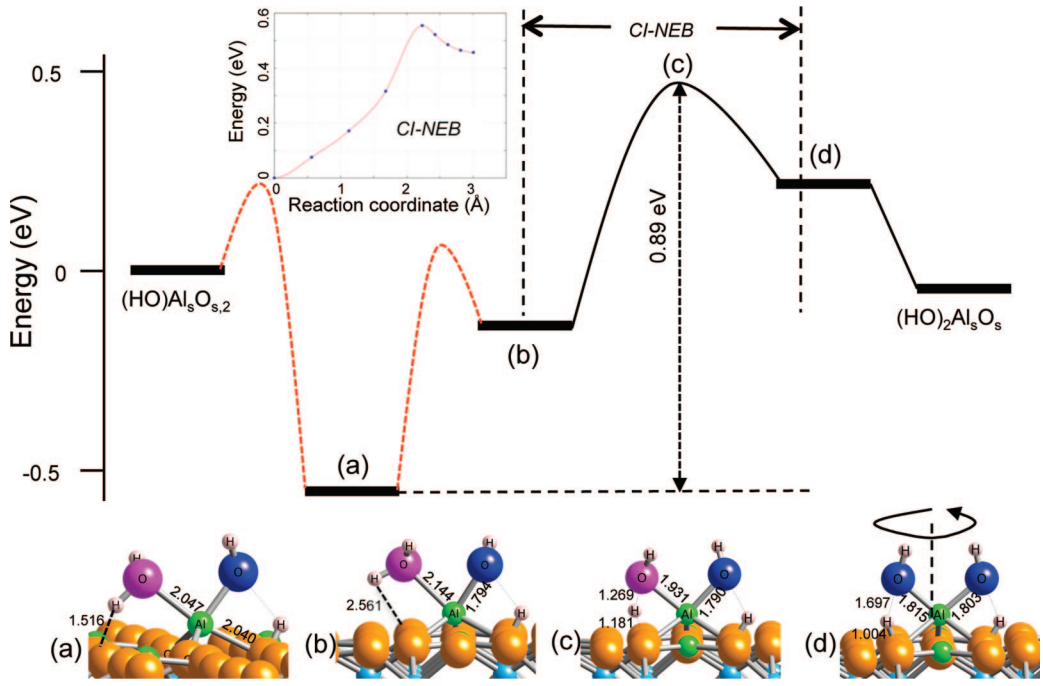

Figure 5. Calculated reaction path for 1,2 water dissociation at a monohydroxylated Al_s. Red dotted curves indicate possibly activated water adsorption and reorientation steps. The solid black curve and inset illustrate the CI-NEB pathway for H−OH bond cleavage. Unscaled $\nu_{TS}^{\ddagger} = 587i$ cm^{-1}.

neighbor O_s. This reorientation costs ≈0.4 eV and, again, although not studied here, could have some (likely small) activation barrier. Similarly, a distorted dihydroxylated state, structure d in Figure 5, is located in the product path. This structure differs from the final product by a twist and Al displacement toward the final, bridge location. CI-NEB calculations succeeded in locating a transition state for H−OH dissociation, structure c, 0.9 eV above the adsorbed water state. The proton-transfer component of the transition state structure is reminiscent of that shown in Figure 4, but increased congestion around Al_s and the smaller reaction energy increase the reaction barrier. Although these results are not sufficient to draw quantitative conclusions about the kinetics of dihydroxyl formation, they strongly suggest that this step is slower than the initial Al_s hydroxylation.

3.3. Final Water Dissociation States. The final step in liberating Al_s from the alumina surface is the dissociation of a third water molecule across the remaining Al_s-O_s bond. Figure 2f shows the product of 1−2 dissociation at a dihydroxylated $(HO)_2Al_sO_s$ site. The formation of a product $Al(OH)_3$ molecule with approximately trigonal coordination about the Al_s center is clearly evident. All three Al−OH bonds are essentially equivalent, and the fragment is displaced upward from the surface and laterally to a location nearly atop one of the protonated O_s sites, with which it retains a longer, dative interaction. As persists in the fully hydroxylated surface, two of the O_s-bound protons point upward from the surface plane, and the third lies in-plane.

The formation energy of an isolated $Al_s(OH)_3$ site with respect to the dry surface and three molecular waters is calculated to be −1.45 eV so that as with the second water addition, the third water addition step is essentially thermoneutral at low coverage.

$$(HO)_2Al_sO_s + H_2O \rightarrow (HO)_3Al_s + O_sH \quad \Delta E_3 = -0.01 \text{ eV} \tag{4}$$

These energetics are again found to be only slightly sensitive to the overall surface hydroxyl coverage. For instance, on a surface containing 3/4 ML of monohydroxylated and 1/4 ML of dihydroxylated sites, the reaction 4 energy becomes +0.2 eV. We examined a variety of coverages of mono-, di-, and trihydroxylated sites in 1/4 ML increments. As noted above, formation of monohydroxylated sites is uniformly exothermic, whereas exact numbers vary with coverage; further hydroxylation via water dissociation proceeds with, at most, a modest thermodynamic driving force; and multiple hydroxylations are uniformly endothermic with respect to adsorbed molecular water.

To identify a minimum energy path for reaction 4, we searched for molecular water adsorbed at a $(HO)_2Al_sO_s$ site. This initial adsorption state is shown on the left side of Figure 6. By comparison with Figure 2e, the adsorbed H_2O molecule is seen to displace the HO_s-Al_s dative bond, leaving a trigonal pyramidal Al_s with only one remaining bond to O_s. This molecular water is bound by −0.57 eV, or again, nearly 0.5 eV more weakly than water in a molecular overlayer. We constructed a candidate reaction pathway to the trihydroxylated $(HO)_3Al_s$ state starting from this point, and CI-NEB calculations converged on a smooth reaction path from the adsorbed water to this final state, shown in Figure 6. This dissociation follows a path in which one of the adsorbed water protons reorients from a more distant O_s toward the nearest neighbor one. At the transition, state this transferring proton is displaced approximately equally from both water oxygen and O_s, and the dissociation barrier rises to 0.9 eV with respect to adsorbed H_2O, approximately the same as the second water dissociation step. Again, the existence of other, lower-energy pathways to trihydroxylated Al_s cannot be excluded (for instance, enlisting multiple H_2O to assist protron transfer), but these results are consistent with such steps' being slower than initial hydroxylation.

As noted previously,[11] the product of successive water dissociations is, thus, an $Al(OH)_3$ overlayer above a fully hydroxylated surface. In fact, crystallites of $Al(OH)_3$ have been identified in scanning tunneling microscopy imaging of the α-$Al_2O_3(0001)$ surface at low water dosings.[41] The fully

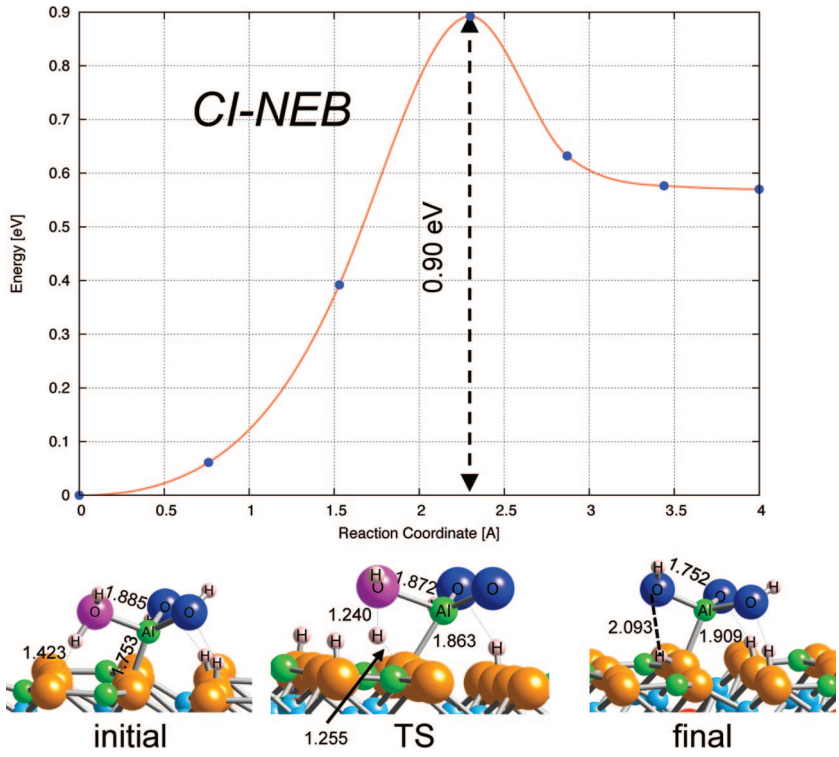

Figure 6. Calculated reaction path for 1,2 water dissociation at a dihydroxylated Al_s. Unscaled $\nu_{TS}^{\ddagger} = 861i$ cm^{-1}.

hydroxylated surface is revealed by removal of this overlayer. We calculate simple removal to the gas phase to be endothermic,

$$(HO)_3Al_s \rightarrow Al(OH)_3(g) \quad \Delta E = +0.84 \text{ eV} \qquad (5)$$

whereas removal via reaction with water is approximately thermoneutral.

$$(HO)_3Al_s + H_2O(g) \rightarrow (H_2O)Al(OH)_3(g) \quad \Delta E = -0.02 \text{ eV} \qquad (6)$$

Comparisons of the surface free energies of various reacted surfaces generally assume that Al liberated from the surface is in equilibrium with bulk Al_2O_3.[11−14,16,29] As we describe more fully below, under this assumption, formation of the fully hydroxylated surface becomes highly favored.

Our calculated structure of the fully hydroxylated surface with the $Al(OH)_3$ removed, obtained by searching over a variety of hydroxyl conformations, is shown in Figure 3d and is similar to previous reports. In particular, the layer of O_s is flat, and 2/3 of the adsorbed hydrogen point out of the surface plane in alternating directions and 1/3 orient within the plane. Forcing the hydroxyls to be uniformally upright costs 0.79 eV/Al_s. Each protonated O_s bridges two underlying Al_s, the latter of which are octahedrally coordinated. As with the dry and Al_s-hydroxylated surfaces, we find the fully hydroxylated surface can accommodate an additional overlayer of molecular water in the form of a hexagonal bilayer (Figure 3e) and that this adsorption has little effect on surface structure. Half of these adsorbed water are found to bind with O atop upright surface hydroxyl groups and half to adsorb perpendicular to the surface with H atop in-plane O_s−H sites. Despite these differing orientations, the water O layer has only a 0.07 Å corrugation. The binding energy of this molecular overlayer on the fully hydroxylated surface is −0.72 eV/H_2O, or 0.4 eV weaker adsorption than on the dry surface, reflecting the difference in binding mechanisms on these two.

The structure of this full hydroxylated, gibbsite-like surface has been determined experimentally using crystal truncation rod diffraction.[23] The overall agreement with the calculated structure is excellent: in addition to agreement in overall surface stoichiometry and exclusive presence of octahedral Al, we find a vertical spacing between O_s and the first Al sublayer of 0.90−0.95 Å, as compared to the reported 1.0 Å, and between first and second Al sublayers of 0.29 Å, as compared to 0.23 Å reported. We find a molecular water overlayer to sit an average of 2.7 Å out of the O_s plane, as compared to 2.3 Å in the experiments, but the presence of significant amounts of carbon in the experimental overlayer may obscure this comparison.

4. Discussion

We have identified here a variety of molecular and dissociated states of water on the α-Al_2O_3(0001) surface. Initial hydroxylation across Al_s−O_s bonds is exothermic, but subsequent hydroxylations are nearly thermoneutral. There have been a number of reports of first principles thermodynamic modeling[42,43] of the relative free energies of various terminations of this basal plane either with or without hydrogen,[11−14,16,29] and it is useful to put the present results on a similar basis. The stoichiometric reactions of the Al-terminated surface with H_2O studied here can all be written as

$$Al_s + xH_2O \rightarrow Al_{s,\theta}H_{3(1-\theta)}(H, OH)_{x-\frac{3}{2}(1-\theta)} + \frac{1}{2}(1-\theta)Al_2O_3(s) \qquad (7)$$

Here, x describes the number of H_2O reacted per Al_s site and runs from 0 to 3, θ is the fraction of Al_s remaining after reaction and is either 0 or 1 in the surfaces we consider, and any Al_s removed from the surface is assumed to be incorporated into bulk Al_2O_3. The change in α-Al_2O_3(0001) surface energy with reaction 7 can be written[43]

$$\Delta\gamma(\theta,x)=\frac{G(\theta,x)-G(1,0)+\frac{1}{2}(1-\theta)G_{Al_2O_3}-x\mu_{H_2O}}{A} \quad (8)$$

where $G(\theta, x)$ and $G(1, 0)$ are the free energies per surface site of a reacted surface and of the dry surface, respectively, $G_{Al_2O_3}$ is the free energy of bulk α-Al_2O_3 per formula unit, μ_{H_2O} is the chemical potential of the H_2O source, and A is the surface area per Al_s site. For the purposes of qualitative comparison, the free energies can be approximated by their respective DFT supercell energies, $G(\theta, x) \approx E(\theta, x)$. Similarly, we can write

$$\mu_{H_2O}=\mu_{H_2O}(0)+\Delta\mu\approx E^{DFT}_{H_2O}+\Delta\mu_{H_2O} \quad (9)$$

where μ_{H_2O} is the chemical potential of water relative to an isolated water molecule at 0 K.

Figure 7 plots $\Delta\gamma$ vs $\Delta\mu$ from eq 8 for the dry surface, the five surface compositions shown in Figure 3, and for a fully dihydroxylated surface, $(HO)_2Al_sO_s$. All of these are taken at unit coverage, because we have found coverage to have a generally small effect on surface energies and the most stable configurations to have unit coverage. The three most prominent free-energy-minimizing, stable surfaces with increasing H_2O potential are the dry surface (Figure 1), the fully hydroxylated (Figure 3d), and the fully hydroxylated with molecular water (Figure 3e). Consistent with earlier reports,[29] the Al_s hydroxylated surface enjoys a narrow window of stability; in this work, near $\Delta\mu_{H_2O} = -1.5$ eV. Molecular water adsorbed on the dry surface, the hydroxylated surface, or the dihydroxylated surface are all seen to be metastable, nonequilibrium configurations. Consistent with the results above, the surface configurations that would seem to connect the dry to the fully hydroxylated surface are high in energy and unlikely to persist. Given the uncertainties in the absolute DFT binding energies and the neglect of finite temperature contributions to G, the exact H_2O temperatures and pressures corresponding to these phase boundaries cannot be determined precisely, but previous estimates place these values in the region of ambient temperatures and water partial pressures.[29]

The results of Figure 7 are predicated on an equilibrium between liberated Al_s and bulk alumina. The ability for liberated Al_s to achieve this equilibrium may be limited under experimental conditions in which, for instance, transport of dissociation products is slow. Further, as found in the MEP calculations above, complete liberation of Al_s by water dissociations is likely much slower than initial water dissociation. The overall picture that emerges for reaction of the α-Al_2O_3(0001) basal plane can be summarized as shown in Figure 8: the hydrogen-free, dry

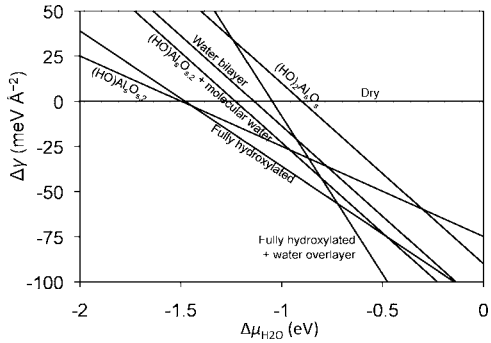

Figure 7. DFT-calculated change in α-Al_2O_3(0001) surface energy vs H_2O chemical potential at saturation coverage of various H_2O reaction products.

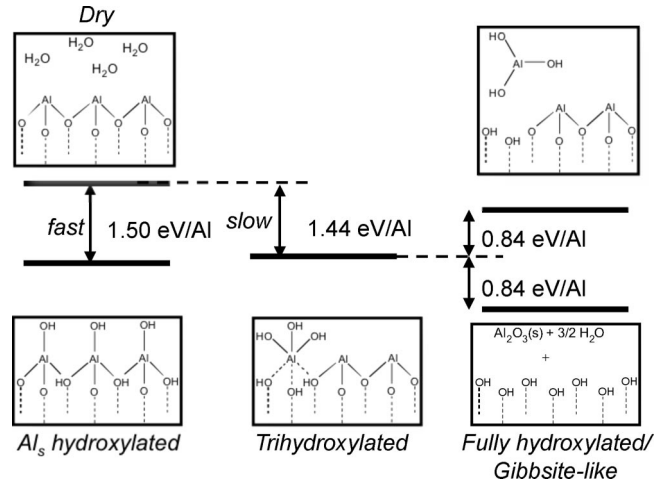

Figure 8. Schematic of overall α-Al_2O_3(0001) reaction landscape.

TABLE 1: Hydroxyl Group Scaled DFT Harmonic Vibrational Frequencies (cm^{-1}) and Hydroxyl Tilt Angles with Respect to the Surface Normal

	frequency	(tilt angle)		
Al_s-hydroxylated	3788 (36°)	3561 (54°)		
fully hydroxylated	3768 (19°)	3710 (32°)	3475 (89°)	
fully hydroxylated + H_2O	3739 (18°)	3410 (9°)	3392 (93°)	3300−2950

surface readily adsorbs and reacts one water per surface Al site with a nearly coverage-independent energy; this surface can adsorb molecular water exothermically, but dissociative adsorption to more highly hydroxylated surface sites has a small thermodynamic driving force and is relatively slow; the energetics of the final removal of fully reacted Al_s depends on the disposition of the hydrated aluminum and could be endo- or exothermic. Once the surface becomes fully hydroxylated, reconstitution of the dry surface proceeds only by transport of Al from the bulk or solution, processes that are likely to have high activation energies.

Microcalorimetry has been used to characterize alumina surface hydration.[17,18,26] The flat energy landscape between the mono- and trihydroxylated surfaces and the dependence of the overall thermodynamics on the fate of surface Al clearly make it difficult to definitively relate observed energetics with specific surface reaction steps. Such correlations remain a challenge to experiment and simulation.

Vibrational spectroscopy offers a means to characterize these various surface hydroxyl groups. Table 1 summarizes DFT-calculated hydroxyl vibrational spectra of the three thermodynamically stable surface compositions from Figure 7. The Al_s hydroxylated surface (Figure 3b) displays two distinct hydroxyl stretches separated by 225 cm^{-1}, the higher frequency corresponding to the more upright Al_s-O-H, and the lower, to the in-plane O_s-H modes. Consistent with the mix of 2/3 out-of-plane and 1/3 in-plane O_s-H groups, the fully hydroxylated surface (Figure 3d) displays three modes: two at higher frequency corresponding to upright O_s-H groups, slightly split due to differences in orientation with respect to the surface normal, and the third at lower frequency, corresponding to O_s-H directed nearly within the surface plane. The splitting of the upright mode frequencies is significantly magnified by adsorption of molecular water (Figure 3e). At monolayer molecular water coverage, water molecules sit directly atop half of the upright O_s-H groups, and these O_s-H stretches become

significantly red-shifted, to ~3400 cm^{-1}. The vibrational frequencies of the "free" O_s−H groups are roughly unperturbed. The adsorbed water modes are calculated to occupy a band of "icelike" frequencies below 3300 cm^{-1}.

Consistent with these results, vibrational spectra of water on single crystal (0001) α-Al_2O_3 do show vibrational modes associated with surface hydroxyls as well as molecular water overlayers that appear to be ordered, even at room temperature.[24,25] Recent sum-frequency vibrational spectroscopy measurements identify a strong hydroxyl peak above 3700 cm^{-1} and a less-intense mode near 3430 cm^{-1} on an α-Al_2O_3(0001) surface exposed to humid air or water.[25] The first of these has been attributed to upright O_s−H vibrations on the fully hydroxylated surface, and comparison with Table 1 supports this assignment. Polarization spectra indicate an O_s−H tilt angle of 26 ± 2°, near the midpoint of the 18−32° degree range found for upright O_s−H here. As shown previously,[21] these hydroxyls are dynamic, and the observed tilt angle is likely a time average over a range of orientations.

The assignment of the 3430 cm^{-1} is not as straightforward. This vibration is near the predicted range of the in-plane O_s−H stretch. However, although the 3700 cm^{-1} mode is observed to persist even upon drying the surface at 600 °C, the lower frequency mode decreases in intensity with drying, suggesting the modes arise from vibrations of adsorbed molecular water.[24,25] The Table 1 results offer another possible interpretation: the 3430 cm^{-1} band is precisely in the range (3410 cm^{-1}) predicted for upright O_s−H hydrogen-bonded to adsorbed water. Such an assignment is consistent with a sensitivity of this mode both to drying and, in the presence of bulk water, to pH.[25]

Finally, it has to be noted that the results reported here are for the undefected and unreconstructed alumina basal plane. Surface defects and long-range reconstructions[41] likely influence the rates of all reactions with water. Although confirmation awaits further simulation, we expect the results reported here to capture the qualitative features of relative reactivity and stability, even in the presence of these complicating factors.

5. Conclusions

Molecular details of the reactions of metal oxides with water are critical to understanding the further surface chemistry of these materials. Here, we have used DFT simulation to examine steps in the adsorption and dissociation of water on the (0001) basal plane of α-Al_2O_3. We find that, although the initial steps in surface hydroxylation are facile and thermodynamically favored, subsequent steps lead to relatively high energy intermediates and, in the reaction paths we have been able to identify, occur with higher activation barriers. Surface coverage is found to have a relatively modest effect on these energetics. The fully hydroxylated, or gibbsite-like, surface is the thermodynamic ground state in the presence of water, and calculations of both the formation energies and vibrational spectrum of this surface are consistent with and assist interpretation of experiments. The reactions leading from the dry to this fully hydroxylated basal surface may depend on mechanisms other than simple water dissociations at surface Al sites. Identification of these intermediate states and steps would be of great value in developing a complete atomistic picture of water reactivity in this important oxide system.

Acknowledgment. The research described herein was supported by the Office of Basic Energy Sciences of the U.S. Department of Energy. This is contribution number 4772 from the Notre Dame Radiation Laboratory. W.F.S. dedicates the manuscript to the memory of Dr. Kenneth C. Hass.

Note Added after ASAP Publication. This article was published ASAP on January 5, 2009. The NDRL number in the Acknowledgment has been changed. The correct version was published on January 8, 2009.

References and Notes

(1) Thiel, P.; Madey, T. *Surf. Sci. Reports* **1987**, *7*, 211–385.
(2) Henrich, V.; Cox, P. *The Surface Science of Metal Oxides*; Cambridge University Press: Cambridge, 1994.
(3) Brown, G., Jr.; Henrich, V.; Casey, W.; Clark, D.; Eggleston, C.; Felmy, A.; Goodman, D.; McCarthy, M.; Maciel, G.; McCarthy, M.; Nealson, K.; Sverjensky, D.; Toney, M.; Zachara, J. *Chem. Rev.* **1999**, *99*, 77–174.
(4) Henderson, M. A. *Surf. Sci. Rep.* **2002**, *46*, 1–308.
(5) Verdaguer, A.; Sacha, G. M.; Bluhm, H.; Salmeron, M. *Chem. Rev.* **2006**, *106*, 1478–1510.
(6) Wefers, K.; Misra, C. *Oxides and hydroxides of Alumina Technical Report*; Alcoa technical paper no. 19, revised; Alcoa Laboratories, Alcoa Center, PA, 1987.
(7) Knözinger, H.; Ratnasamy, P. *Catal. Rev.-Sci. Eng.* **1978**, *17*, 31–70.
(8) Wyckoff, R. *Crystal Structures*; Interscience: New York, 1963; Vol. 1−6.
(9) Ahn, J.; Rabalais, J. W. *Surf. Sci.* **1997**, *388*, 121–131.
(10) Guo, J.; Ellis, D. E.; Lam, D. J. *Phys. Rev. B* **1992**, *45*, 13647.
(11) Di Felice, R.; Northrup, J. *Phys. Rev. B* **1999**, *60*, R16287.
(12) Batyrev, I.; Alavi, A.; Finnis, M. *Faraday Discuss.* **1999**, *114*, 33–43.
(13) Wang, X. G.; Chaka, A.; Scheffler, M. *Phys. Rev. Lett.* **2000**, *84*, 3650–3653.
(14) Tepesch, P.; Quong, A. *Phys. Status Solidi* **2000**, *217*, 377.
(15) Soares, E. A.; Van Hove, M. A.; Walters, C. F.; McCarty, K. F. *Phys. Rev. B* **2002**, *65*, 195405.
(16) Marmier, A.; Parker, S. C. *Phys. Rev. B* **2004**, *69*, 115409.
(17) McHale, J.; Auroux, A.; Perrotta, A.; Navrotsky, A. *Science* **1997**, *277*, 788.
(18) McHale, J.; Navrotsky, A.; Perrotta, A. *J. Phys. Chem. B* **1997**, *101*, 603–613.
(19) Elam, J.; Nelson, C.; Cameron, M.; Tolbert, M.; George, S. *J. Phys. Chem. B* **1998**, *102*, 7008–7015.
(20) Liu, P.; Kendelewicz, T.; Brown, G. E.; Nelson, E. J.; Chambers, S. A. *Surf. Sci.* **1998**, *417*, 53–65.
(21) Hass, K. C.; Schneider, W. F.; Curioni, A.; Andreoni, W. *Science* **1998**, *282*, 265–268.
(22) Hass, K. C.; Schneider, W. F.; Curioni, A.; Andreoni, W. *J. Phys. Chem. B* **2000**, *104*, 5527–5540.
(23) Eng, P. J.; Trainor, T. P.; Brown, G. E.; Waychunas, G. A.; Newville, M.; Sutton, S. R.; Rivers, M. L. *Science* **2000**, *288*, 1029–1033.
(24) Al-Abadleh, H. A.; Grassian, V. H. *Langmuir* **2003**, *19*, 341–347.
(25) Zhang, L.; Tian, C.; Waychunas, G. A.; Shen, Y. R. *J. Am. Chem. Soc.* **2008**, *130* (24), 7686–7694.
(26) Rossi, P.; Oliveri, G.; Bassoli, M. *J. Chem. Soc., Faraday Trans.* **1994**, *90*, 363–367.
(27) Wittbrodt, J.; Hase, W.; Schlegel, H. *J. Phys. Chem. B* **1998**, *102*, 6539.
(28) Shapovalov, V.; Truong, T. *J. Phys. Chem. B* **2000**, *104*, 9859.
(29) Łodziana, Z.; Nørskov, J. K.; Stoltze, P. *J. Chem. Phys.* **2003**, *118*, 11179–11188.
(30) Kresse, G.; Hafner, J. *Phys. Rev. B* **1994**, *49*, 14251.
(31) Kresse, G.; Furthmuller, J. *Phys. Rev. B* **1996**, *54*, 11169–11186.
(32) Perdew, J. P.; Chevary, J. A.; Vosko, S. H.; Jackson, K. A.; Pederson, M. R.; Singh, D. J.; Fiolhais, C. *Phys. Rev. B* **1992**, *46*, 6671–6687.
(33) Blöchl, P. *Phys. Rev. B* **1994**, *50*, 17953–17979.
(34) Kresse, G.; Joubert, J. *Phys. Rev. B* **1999**, *59*, 1758–1775.
(35) Ranea, V. A.; Schneider, W. F.; Carmichael, I. *Surf. Sci.* **2008**, *602*, 268–275.
(36) Henkelman, G.; Uberuaga, B. P.; Jónsson, H. *J. Chem. Phys.* **2000**, *113*, 9901–9904.
(37) Jónsson, H.; Mills, G.; Jacobsen, K. In *Classical and Quantum Dynamics in Condensed Phased Simulations*; Berne, B., Ciccotti, G., Coker, D., Eds.; World Scientific: River Edge, NJ , 1998; pp 389−405.
(38) Scott, A.; Radom, L. *J. Phys. Chem.* **1996**, *100*, 16502.
(39) Schneider, W.; Hass, K.; Miletic, M.; Gland, J. *J. Phys. Chem. B* **2002**, *106*, 7405–7413.
(40) Schneider, W. *J. Phys. Chem. B* **2004**, *108*, 273–282.

(41) Barth, C.; Reichling, M. *Nature* **2001**, *414*, 54–57.
(42) Reuter, K.; Stampfl, C.; Scheffler, M. Fundamental Models and Methods. In *Handbook of Materials Modeling*; Yip, S., Ed.; Springer: Berlin, 2005; Vol. 1.
(43) Getman, R. B.; Xu, Y.; Schneider, W. F. *J. Phys. Chem. C* **2008**, *112*, 9559–9572.

JP8069892